

Electro-Optic Modulator source as sample-free calibrator and frequency stabilizer for Brillouin Microscopy

Claudia Testi^{1*}, Emanuele Pontecorvo^{1,2}, Chiara Bartoli³, Chiara Marzaro¹, Fabrizio Gala^{1,2}, Li Zhang¹, Giulia Zanini^{1,2} and Giancarlo Ruocco^{1,3}

1: Center for Life Nano- and Neuro-Science, Istituto Italiano di Tecnologia, Viale Regina Elena 291, 00161, Roma, Italy

2: CrestOptics S.p.A., Via Di Torre Rossa, 66, 00165, Roma, Italy

3: Dipartimento Di Fisica, Università Di Roma "La Sapienza", Piazzale Aldo Moro, 5, 00185, Roma, Italy

*: *corresponding author: claudia.testi@iit.it*

Abstract

Brillouin Microscopy is a novel label-free optical technique that enables the measurement of a material's mechanical properties at the sub-micron scale in a non-invasive and non-contact way; in the last few years, its applications in the life sciences have extensively expanded. To date, many custom-built Brillouin Microscopes suffer from temporal instabilities that impact their performances, showing drifts in the acquired spectra during time that may lead to inconsistencies between data acquired at different days. A further challenge for standard Brillouin Microscopes is the calibration of the spectrometer: the currently accepted protocol in literature uses known Brillouin shifts of water and methanol to reconstruct the dispersion curve, but this approach is highly influenced by external factors that are unrelated to spectrometer's performances. Manual and frequent realignments of the spectrometer and repeated calibrations with standard materials are thus needed to address these issues.

Here, we show an innovative method to remove temporal instabilities of a standard Brillouin Microscope by inserting an Electro-Optic Modulator (EOM) that can be used: *i*) as a reference signal during measurements; *ii*) as a calibrator, allowing the reconstruction of the spectrometer dispersion curve with high precision, in an automatic pipeline and without the need for reference samples; *iii*) as a tool to detect and compensate for temporal drifts through a feedback control in a closed loop. We here show that our Brillouin Microscope, equipped with an EOM and a tuneable laser, is able to automatically acquire data for more than 2 days without the need to realign the spectrometer; retrieved Brillouin shifts and widths showed superior stability in time than standard Brillouin Microscopes. These results pave the way for a prototype of an automatic Brillouin Microscope that, once aligned, can automatically acquire data for hours or even days.

1. Introduction

Brillouin Microscopy (BM) is a label-free optical technique that enables the measurement of a material's mechanical properties at the sub-micron scale in a non-invasive and non-contact way (Handler et al., 2024). In recent years, its applications in the life sciences have expanded significantly, driven by the growing understanding of how mechanical properties influence biological processes. This advancement allows for the study of biological samples and integrates seamlessly with confocal fluorescence microscopy (Kabakova et al., 2024; Scarcelli et al., 2015; Zhang & Scarcelli, 2021).

This cutting-edge imaging technique provides a complete characterization of the viscoelastic properties of a sample through the analysis of its Brillouin spectra. From the Brillouin spectrum of a material (**Figure 1A, upper panel**) it is possible to quantify its complex Longitudinal Modulus M , composed of a real part (M'), representing the elastic response, and an imaginary part (M''), representing the dissipative response of the material to an external perturbation. This spectrum arises from the scattering of photons upon interaction with the sample's longitudinal acoustic phonons: it consists of a central Rayleigh peak, due to photons scattered at the same frequency of the incident radiation, and two Brillouin peaks, due to photons scattered at lower (Stokes) and higher (Anti-stokes) frequencies than the incident one. These peaks are identical, located in the GHz range, centered around the Brillouin frequency shift ν_B (directly dependent on M' , shown as red dotted lines in **Figure 1A**) and characterized by an equal full width at half maximum (FWHM) Γ_B (directly dependent on M'' , shown as blue arrows in **Figure 1A**). Applications of Brillouin microscopy are emerging in the mechanobiology field to assess biomechanical parameters of cells (D'Annunzio et al., 2024; Fasciani et al., 2020; Scarcelli et al., 2015; Testi et al., 2021) and tissues (D'Annunzio et al., 2024; Martinez-Vidal et al., 2024) under physiological and pathological conditions, highlighting its potential diagnostic use. Modern optical setups that allow for fast and accurate acquisition of Brillouin spectra typically require a VIPA (Virtually Imaged Phase Array), an interferometer that spatially separates the stronger Rayleigh signal from the much weaker Brillouin: a pure Brillouin triplet acquired with a VIPA is thus repeated through different dispersion orders, separated by its FSR (Free Spectral Range), resulting in a spectrum like the one depicted in **Figure 1A lower panel**.

The aim of this study is to introduce technological improvements to overcome major criticalities found in many VIPA-based spectrometers custom-built for BM. State-of-the-art Brillouin spectrometers normally comprise either: *i*) a 532 nm or 660 nm lasers and a double-VIPA scheme, where the parasitic Rayleigh signal is blocked from slits in the spectrometer and only the Brillouin Stokes and Anti-Stokes are present in the data acquisition; or *ii*) a 780 nm laser equipped with a single VIPA scheme and a Rubidium cell that partially absorbs the unwanted Rayleigh line. These lasers are continuous wave,

single-mode, narrow line-width and, importantly, should be stable in time; however, most of the lasers normally used in BM exhibit frequency drifts caused by temperature fluctuations of the room, that negatively affect the performances of long Brillouin acquisitions on biological samples (Zhang & Scarcelli, 2021).

To quantify this frequency shift in time, we evaluated the effects of small temperature changes in our laboratory on a continuous-wave 532 nm laser: at time = 0 we aligned our custom-built spectrometer (here constituted by a double-VIPA scheme with FSR = 30 GHz) to the signal of water, that correctly showed the presence of 2 Brillouin peaks of equal intensity in the camera region of interest (**Figure 1B**, blue spectrum of first panel). Small (<1°C) temperature fluctuations of the room during the acquisitions (**Figure 1B**, **second panel**), however, caused the Brillouin spectra to move considerably (red and yellow spectra of **Figure 1B**, **first panel**, taken after 30' and 60' from the spectrometer manual alignment). Upon such significant drifts of the spectra, the spectrometer calibration performed at the start of the experiment became invalid: as a result, both v_B and Γ_B in just 1 hour fluctuated of nearly 100 MHz (i.e. an oscillation of 1.33%, **Figure 1B**, **third panel**), without any meaningful correlation to the sample temperature, which was kept constant throughout the experiment. In state-of-the-art Brillouin Microscopes for biological applications, the required precision for v_B is set to 10 MHz (Zhang & Scarcelli, 2021): v_B should thus not fluctuate more than 0.1% of its value, and a fluctuation > 1% should be considered as highly impacting on the instrument performance. This drift, moreover, allowed the Rayleigh signal to appear at the edge of the camera region of interest (yellow and red spectra of the first panel), resulting in intensity saturation with potential damage of the camera. Consequently, after just 30-60 minutes from the alignment, data acquisition had to be stopped, the spectrometer realigned and a new calibration acquired.

A possible way to avoid temperature-induced laser frequency shifts is to use laser sources locked to a fixed reference, that by definition do not drift in frequency with temperature. However, also in this case, Brillouin spectra of water performed with our 780 nm locked laser (equipped with a ⁸⁵Rubidium cell and a 1 stage VIPA spectrometer) experienced frequency drifts (**Figure 1C**, **first panel**) by room temperature changes (**Figure 1C**, **second panel**); here, these changes could act only on the VIPA, whose thermal expansions of the cavity caused small variations in Rayleigh position and FSR (**Figure 1C**, **third panel**), resulting in drifts of v_B and Γ_B (**Figure 1C**, **fourth panel**) that, although slower than the non-locked laser (≈ 200 MHz in 3.5 hours for v_B) negatively affected the stability of the spectrometer and showed the need of more frequent spectrometer calibrations.

Another major critical point of a standard BM consists in the pixel-to-GHz calibration of the spectrometer: this is a critical step to perform at the beginning of an experiment and should allow to retrieve the Brillouin shift and FWHM with high precision.

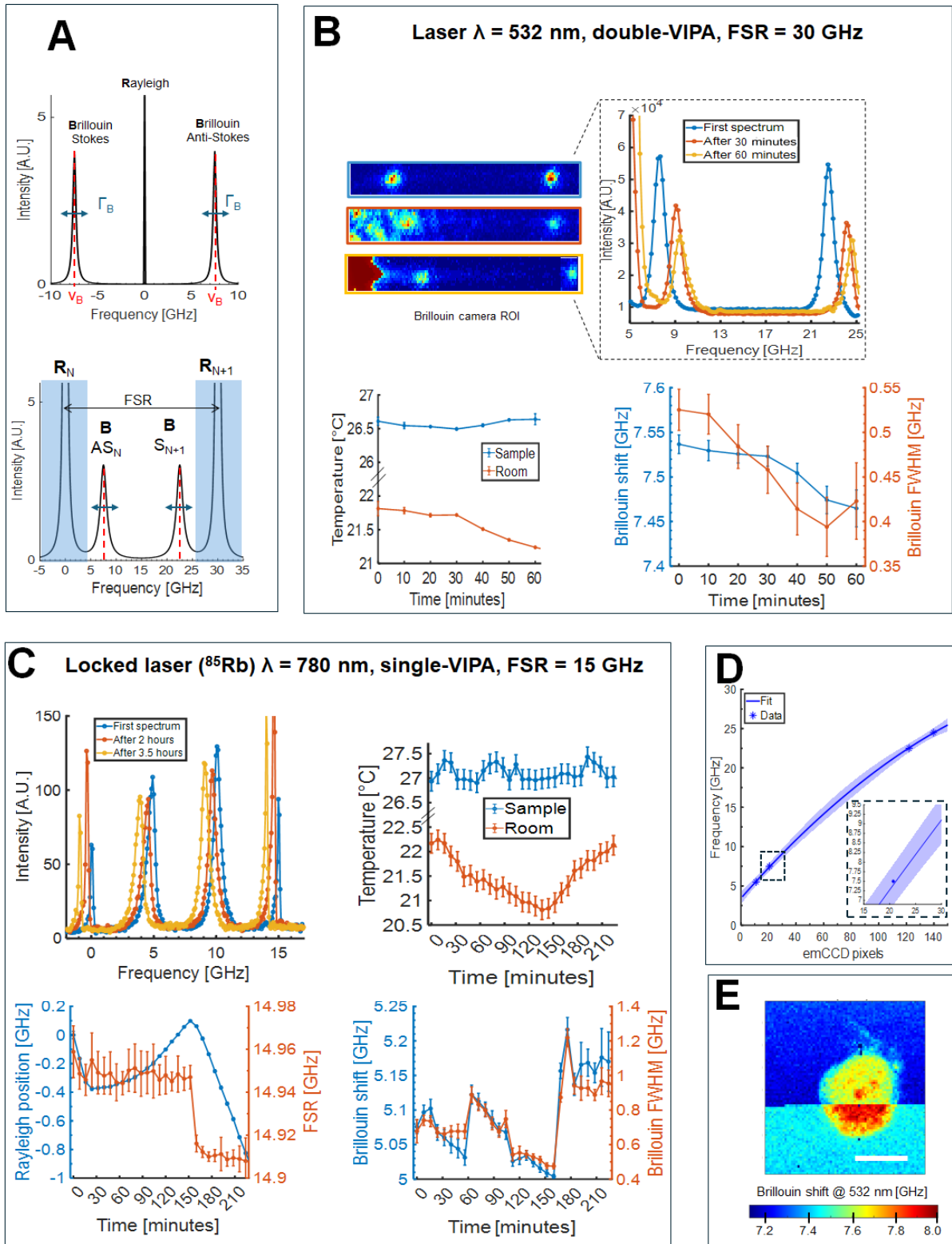


Figure 1: Room temperature changes impact lasers and VIPAs frequency stability, resulting in Brillouin spectra drifts during time. **A:** *top panel:* typical Brillouin spectrum of a material, constituted by a central narrow Rayleigh peak and two side (Stokes and Anti-Stokes) Brillouin peaks: these peaks are centered around the Brillouin frequency shift (ν_B , red dotted lines) and characterized by an equal full width at half maximum (Γ_B , blue arrows). *Lower panel:* Brillouin triplet imaged with a VIPA interferometer, having dispersion orders N (together with its Brillouin Anti-Stokes curve) and $N+1$ (with its Brillouin Stokes curve); the difference in frequency between the order $N+1$ and N is equal to the Free Spectral Range (FSR) of the VIPA. In a double-VIPA setup, the Rayleigh lines are cut out (shaded blue rectangles) and only the Brillouin signals are present during data acquisition. **B:** water data acquired at different times

with 532 nm laser and double-VIPA setup (FSR=30 GHz). *First panel*: behaviour in time of Brillouin water spectra: $t=0$ is the time at which spectrometer alignment has been performed, resulting in a Brillouin spectrum having 2 peaks of equal intensity (blue box and spectrum); because of small room temperature changes, this spectrum drifts in time, until camera saturation occurs as the parasitic Rayleigh line enters in the Brillouin camera ROI (yellow box and spectrum). *Second panel*: temperature of the room, showing slight changes during time, and the sample, whose temperature was kept constant with an incubator. *Third panel*: behaviour of water v_B and Γ_B : a Brillouin measurement was performed every 10', where we acquired 500 spectra and averaged them. Because of frequency drifts and spectral distortion, water Brillouin shifts and FWHMs changed in time although the sample temperature was kept constant. **C**: water data acquired at different times with 780 nm laser, locked at ^{85}Rb , and a single-VIPA spectrometer (FSR=15 GHz). *First panel*: behaviour in time of Brillouin spectra, showing the same drifts as in B; also here, $t=0$ is the time at which spectrometer alignment has been performed. *Second panel*: room and sample temperature behaviour; also here, the sample temperature was kept constant with an incubator. *Third panel*: Rayleigh position and FSR behaviour of the single VIPA during time. Because of room temperature drifts, that here could only affect the VIPA, the Brillouin spectra (first panel), elastic Rayleigh position and FSR (third panel) all shifted during time, resulting in a non-constant water v_B and Γ_B (*fourth panel*). **D**: standard protocol for Brillouin spectrometer pixel-to-GHz calibration, done by taking water and methanol Brillouin spectra pixels positions and imposing their shift to be equal to their known values (Water: 7.5 GHz, Methanol: 5.5 GHz, blue stars). The continuous line represents the fit of the curve obtained with a 2nd order polynomial; shaded area is the 99% confidence interval. In the *dotted box*, close-up of the pixel-to-GHz calibration curve in the region of interest for biological applications, i.e. 7.5-9.5 GHz. **E**: in a double-VIPA setup, a fixed reference as a Rayleigh line is missing: thus, elevated frequency drifts may lead to significant shifts of v_B map during long acquisitions of biological materials. Here we show the Brillouin map of a HeLa cell that shifts in time. Scale bar = 5 microns. All data are shown as mean \pm standard deviation (SD) performed over 500 repeated measurements acquired at a single time; time = 0 refers to the manual alignment of the spectrometer, where Brillouin peaks have the same height.

The currently accepted protocol in literature to calibrate a Brillouin spectrometer is based on the known Brillouin shifts of water and methanol, from which the dispersion curve of the VIPA can be fitted (**Figure 1D**) (Zhang & Scarcelli, 2021). However, this strategy is deeply dependent from factors that are external from the spectrometer performances, since the reference materials v_B might be affected by factors like temperature, pureness, hydration level, physical/chemical composition, or the NA of the objective used (as shown in **Supplementary Figure S1**): as such, the Brillouin shift used as a reference for this critical step is actually not known with the required precision.

The difference of Brillouin shift in biological samples is typically in a restricted range: when using a 532 nm laser, as in our case, a cell map varies between 7.4 to 8.0 GHz, and even a 100 MHz shift due to temperature changes (affecting the instrument or the calibration materials or both) may lead to dis-interpretation of the results. If the desired stability is not reached, frequency drifts may lead to significant shifts of v_B map during long acquisitions, especially in the case of double-VIPA setups where a fixed reference as Rayleigh line is missing (**Figure 1E**), or on datasets that extend over a long period of time, where data consistency across different experimental days becomes crucial.

To overcome these problems concerning sample-dependent calibration and instrumental stability, we inserted in an existing Brillouin Microscope an Electro-Optic Modulator (EOM) (Pontecorvo, 2024) and switched the laser source to a tuneable one, where the laser frequency could be tuned in the GHz range: we obtained a Brillouin microscope stable in frequency for hours or even days and that was not exposed to unavoidable temperature changes of the room. This was possible through a feedback

control in a closed loop governed via MATLAB: in such a manner, we managed to compensate for frequency drifts by taking an EOM signal as a fixed reference during measurements and shifting the laser frequency accordingly, while performing accurate pixel-to-GHz spectrometer calibrations by sending EOM frequencies known with high precision. This calibration method is independent from samples or temperature fluctuations and can also be integrated into an automatic data acquisition pipeline, leading to a significantly more accurate reconstruction of the VIPA dispersion curve. These results pave the way for a prototype of an automatic Brillouin Microscope that, once aligned, can acquire data for hours or days without the need for spectrometer re-alignment and that could be used also by non-expert users.

2. Results & Discussion

2.a Implementation of the EOM source in an existing Brillouin Microscope

Figure 2A shows the launch, source modulation and collection layout of the Brillouin Microscope implemented with an EOM source. We used a single mode laser (Oxxius LCX, $\lambda=532\text{nm}$ wavelength) as the source; most of it is sent to the sample through a polarizing beam splitter (PBS), while a small part is launched into a fiber-integrated phase-modulated EOM.

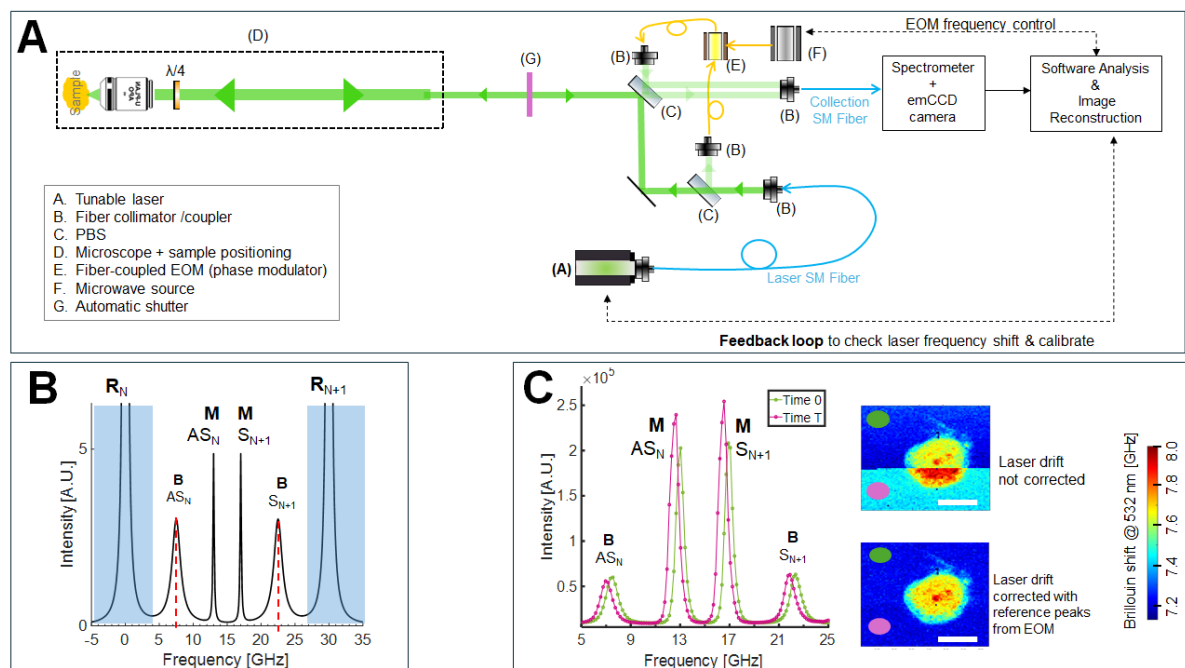


Figure 2: Implementation of an EOM source in an existing Brillouin Microscope. A: launch, source modulation and collection layout of the Brillouin Microscope implemented with an Electro-optic Modulator (EOM) source. We used a single mode, continuous wave, tuneable laser (element (A): Oxxius LCX, $\lambda=532\text{nm}$) as source, coming out from

a single mode (SM) fiber and a collimator (B); most of the laser signal is sent to the sample through a polarizing beam splitter (C) (PBS), while a small part is picked up and launched to the fiber-integrated EOM (yellow lines and boxes, E) through a collimator (B). The inputs to the EOM (E) are the laser signal and a microwave source (F); its output is an optical signal shifted in frequency from 0 to 15 GHz, injected through another collimator and a PBS into the collection fiber (single-mode, ensuring the confocality of the Brillouin Microscope). In the same collection fiber, the Brillouin signal coming from the sample is also collected: this signal comes from (D), along with other optical elements that allow the laser scanning required for Brillouin Microscopy. An automatic shutter (G) blocks the signal coming from the sample and allows for automatic calibration of the system during data acquisition, without interference from the Brillouin signal of the sample. At the end of the collection fiber, the spectrometer (here made by double-VIPA scheme) and a emCCD camera acquire the Brillouin spectra. The setup is governed by a MATLAB code that, together with data acquisitions, performs the feedback control in a closed loop, that moves the laser frequency shift, calibrates and governs the EOM frequency. **B:** sketch of a Brillouin spectrum of water obtained when the EOM is switched on: (B) are Brillouin signals from the samples, (M) are the EOM Anti-Stokes and Stokes signals, visible at ν_{EOM} and $\text{FSR} - \nu_{EOM}$ respectively. Here, we chose $\nu_{EOM} = 13$ GHz as this frequency and its second harmonics are far from frequencies of interest of biological materials (i.e. 7.5-9.5 GHz at 532 nm wavelength). In such a way, the EOM peaks act as a reference, replacing the one missing from Rayleigh's (shaded blue rectangles). **C:** experimental water Brillouin spectrum obtained with the EOM set to $\nu_{EOM} = 13$ GHz. The EOM frequency allows for a quantification of the frequency drifts visible in the acquisitions (green and pink spectra, acquired at different times in the same HeLa cell acquired with our Brillouin Microscope, shown on the right), allowing to compensate it in the Brillouin shift maps.

The EOM is constituted by a crystal that takes the laser signal in input and modulates it with an electric field given by a microwave source, thus giving as output an optical signal shifted in frequency from 0 to 15 GHz from the carrier (elastic light). This output is injected in the collection fiber via another PBS. In the same collection fiber, the Brillouin scattering signal coming back from the sample is also collected; this fiber has the double role to clean the spatial mode sent to the spectrum analyser and to assure the confocality of the laser scanning system. The collected signal, consisting of the sample and EOM Brillouin spectra outputs, is delivered to the spectrum analyser, which in our case is based on a double-VIPA layout (Zhang & Scarcelli, 2021). The whole instrument is governed by a MATLAB software that allowed for image reconstruction, controlled the EOM frequency and performed automatic pixel-to-GHz calibrations. This custom-built MATLAB routine was part of a feedback control in a closed loop that compensated for temperature-induced frequency drifts by moving back the laser wavelength upon checking the position of the absolute EOM signals; after that, the routine automatically performed pixel-to-GHz calibration to adjust for possible changes in the FSR of the spectrometer (Pontecorvo, 2024).

Firstly, we wanted to deal with the missing reference of a double-VIPA scheme, where the Rayleigh line is cut out, in order to quantify the drift of Brillouin spectra in time. To achieve this, we used the EOM frequency as a reference peak replacing the Rayleigh line: the EOM peaks, in fact, could be placed anywhere within the Gaussian envelope of the VIPA transmission, allowing for high flexibility during different measurements. **Figure 2B** shows a sketch of the resulting Brillouin data when the EOM is switched on and its frequency set to 13 GHz: those marked by (B) correspond to sample's Stokes and Anti-Stokes Brillouin signals, respectively coming from two subsequent orders of the VIPA response, while those marked by (M) come from the EOM; the elastic Rayleigh signal is

blocked by the slits in the spectrometer (shown as blue shaded rectangles). We chose $\nu_{\text{EOM}} = 13$ GHz because this frequency, its Stokes (located at $\text{FSR} - \nu_{\text{EOM}}$) and its second harmonics (located at $2*\nu_{\text{EOM}}=26$ GHz and $\text{FSR}- 2*\nu_{\text{EOM}}=4$ GHz, not visible in the frequency range 5-25 GHz) do not overlap with the Brillouin signals coming from the biological materials (i.e. 7.5-9.5 GHz at 532 nm).

A typical experimental Brillouin spectrum of water acquired with our setup is shown in **Figure 2C, left**: the spectrum had 4 peaks, i.e. 2 Brillouin peaks from the sample (the Anti-Stokes at 7.5 GHz and the Stokes at $\text{FSR}-7.5 = 22.5$ GHz) and 2 from the EOM (the Anti-Stokes at 13 GHz and the Stokes at $\text{FSR}-13=17$ GHz). Upon drifts of the Brillouin spectra, the (M) peak can be used as reference, thus quantifying the drift in frequency and compensating for laser drifts during long acquisitions of biological samples (**Figure 2C, right**). From the difference between the EOM Stokes and Anti-Stokes positions, moreover, it was possible to quantify the FSR and characterize its behaviour during time.

These results show that the EOM can act as a reference signal, replacing the missing Rayleigh lines in a double-VIPA spectrometer and allowing for the quantification of the unavoidable temperature-induced frequency drifts; its frequency ν_{EOM} does not overlap with the Brillouin signals in the frequencies of interest for biological materials and, consequently, this signal does not alter the data acquisition.

2b. EOM source as a sample-free calibrator

Next, we sought to find a new strategy for pixel-to-GHz calibration in a sample-free manner by using reliable frequency signals coming from the EOM. When sending a single frequency to the EOM microwave generator (for example, $\nu_{\text{EOM}} = 7$ GHz as in **Figure 3A, top panel**), the output on the camera of the spectrometer was constituted by 4 peaks: the first two were the fundamental frequency and its second harmonic (i.e. ν_{EOM} and $2*\nu_{\text{EOM}}$, here 7 GHz and 14 GHz), while the other two were their respective Stokes peaks (i.e. $\text{FSR}-\nu_{\text{EOM}}$ and $\text{FSR}-2*\nu_{\text{EOM}}$, here 23 GHz and 16 GHz when using $\text{FSR} = 30$ GHz). In such a manner, from a single EOM frequency we could obtain two information with high precision: one relative to the VIPA dispersion curve and one relative to the real FSR value. In order to reconstruct the calibration curve with more accuracy by adding data points, we tuned the microwave generator at 7, 8.7, 10.9 and 11.5 GHz, thus obtaining a total of 16 peaks from the resulting curves (**Figure 3A, lower panel**). These values were chosen because in our setup their Stokes and Anti-Stokes did not overlap and, importantly, their extent covered the whole range of frequencies of interest for biological applications, whose Brillouin shifts with 532 nm laser span between 7.5 to 8 GHz in cells (D'Annunzio et al., 2024; Handler et al., 2024; Testi et al., 2021) and between 7.5 to 9.5 GHz in tissues (Martinez-Vidal et al., 2024).

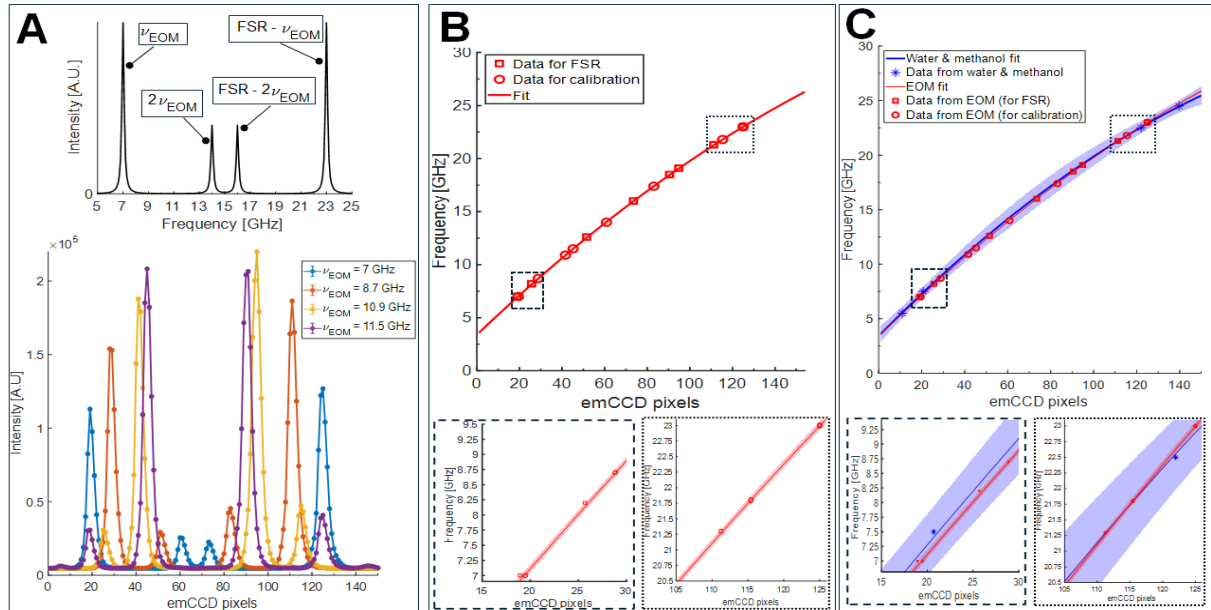


Figure 3: EOM source can be used as a reference-free pixel-to-GHz calibration of Brillouin spectrometers. A: upper panel: output of a single EOM frequency when its second harmonics are visible and no Brillouin signal comes from the sample (the shutter of Figure 2A is activated). Here, we sent $\nu_{EOM} = 7$ GHz; the output at the camera spectrometer were 4 peaks at ν_{EOM} , $2\nu_{EOM}$, $FSR - 2\nu_{EOM}$, $FSR - \nu_{EOM}$ (located at 7, 14, 16 and 23 GHz respectively). **Lower panel:** EOM spectra used for pixel-to-GHz calibration purposes, coming from $\nu_{EOM} = 7$ GHz (blue spectrum), $\nu_{EOM} = 8.7$ GHz (red), $\nu_{EOM} = 10.9$ GHz (yellow) and $\nu_{EOM} = 11.5$ GHz (purple). **B:** from the spectra of A, we had a total of 16 datapoints to calibrate the spectrometer. The continuous line is the 2nd order polynomial fit of the pixel-to-GHz calibration curve; shaded areas show 99% confidence intervals of the fit. Rectangle inserts show the fit accuracy in the frequencies of interest for biological applications (7.5-9.5 GHz and their Stokes counterpart 20.5-22.5 GHz). **C:** comparison of EOM obtained dispersion curve (red datapoints, line and shaded areas) with the one obtained from the standard protocol from water and methanol Brillouin shifts (blue datapoints, line and shaded areas) coming from Figure 1D. All the shaded areas show 99% confidence intervals of the 2nd order polynomial fit: errors made with our EOM method are much lower than the standard protocol in all the frequencies and especially in the frequencies of interest.

Their pixel-to-frequency curve is shown in **Figure 3B**, where we used 8 points (circles datapoints in the figure) for the determination of the coefficients of the 2nd order polynomial. This procedure had an outstanding precision in determining the pixel-to-GHz relation, particularly in the frequencies of interest for Brillouin Microscopy, i.e. in our case 7.5-9.5 GHz (**left box of Figure 3B**) and its Stokes counterpart 20.5-22.5 GHz (**right box of Figure 3B**): resulting frequencies were obtained with an error of the order of ≈ 10 MHz. This novel calibration protocol, moreover, was incredibly fast (less than 10 seconds were needed to obtain all the curve here showed) and could be programmed in the data acquisition routine in order to automatically calibrate every fixed amount of time. If more precision is required, additional frequencies can be added to the calibration curve at any desired location.

In **Figure 3C** we compared the calibration curve obtained from the 8 data points using the EOM (red datapoints, curve and shaded area) with the curve obtained from the standard calibration protocol with water and methanol Brillouin shifts (Zhang & Scarcelli, 2021), obtained from 4 data points (blue datapoints, curve and shaded area; the points are

located at $\nu_{\text{water}} = 7.5$ and 22.5 GHz and $\nu_{\text{methanol}} = 5.5$ and 24.5 GHz, assuming a constant FSR = 30 GHz and Brillouin shifts values known from theoretical calculations, that however are also dependent from the objective, as shown in **Supplementary Figure S1**. Shaded areas under the curves represent the errors in the reconstruction of each 2nd order polynomial with 99% confidence intervals (equal to 3σ): even if all the datapoints lied on the same curve, the red areas were narrower, corresponding to much higher precision in reconstructing the Brillouin shifts in the regions of interest for biological applications (i.e. 2 MHz precision with EOM vs 100 MHz precision with water and methanol, left and right box inserts of **Figure 3C**).

In sum, the calibration protocol of our Brillouin Microscope equipped with an EOM source is completely independent from reference samples (subjected to room temperature changes or to different physical-chemical compositions) or the objective used: its pixel-to-GHz calibration curve is only a property of the spectrometer alignment, which can differ on a day-to-day basis. This procedure is very precise, fast and automatic. It can be used to calibrate pixel-to-GHz dispersion curves of spectrometers regardless of their specific components and is thus suitable for single-VIPA or double-VIPA or even Tandem Fabry-Perot setups.

2c. High stability of the EOM-equipped Brillouin Microscope in time with a tuneable laser source

We next wanted to remove significant Brillouin spectra drifts during time (**Figure 4A, first panel**, where we show Brillouin spectra of water with the EOM inserted, taken at different times from the spectrometer alignment). As said, these drifts are caused by small temperature changes in the laboratory (**Figure 4A, second panel**) that affect either laser frequency stability, or the thermal expansions of the VIPA cavity, or both: if the acquisition is not stopped, in a double-VIPA configuration eventually a lot of spurious background due to the unblocked Rayleigh peak enters in the window of interest, thus saturating the signal and negatively affecting the measurements of ν_B and Γ_B (**Figure 4A, third panel**). Here, laser drifts accumulated dramatically over time: the EOM reference moved considerably from the initial position (for a total of 1.5 GHz in 100', i.e. a change of $\approx 12\%$, **Figure 4A, fourth panel**), while the FSR showed a high dependency from the external room temperature (**Figure 4A, fifth panel**). Consequently, after just 100 minutes from the alignment, data acquisition had to be stopped and the spectrometer had to be manually realigned to overcome camera saturation caused by the unfiltered Rayleigh signal.

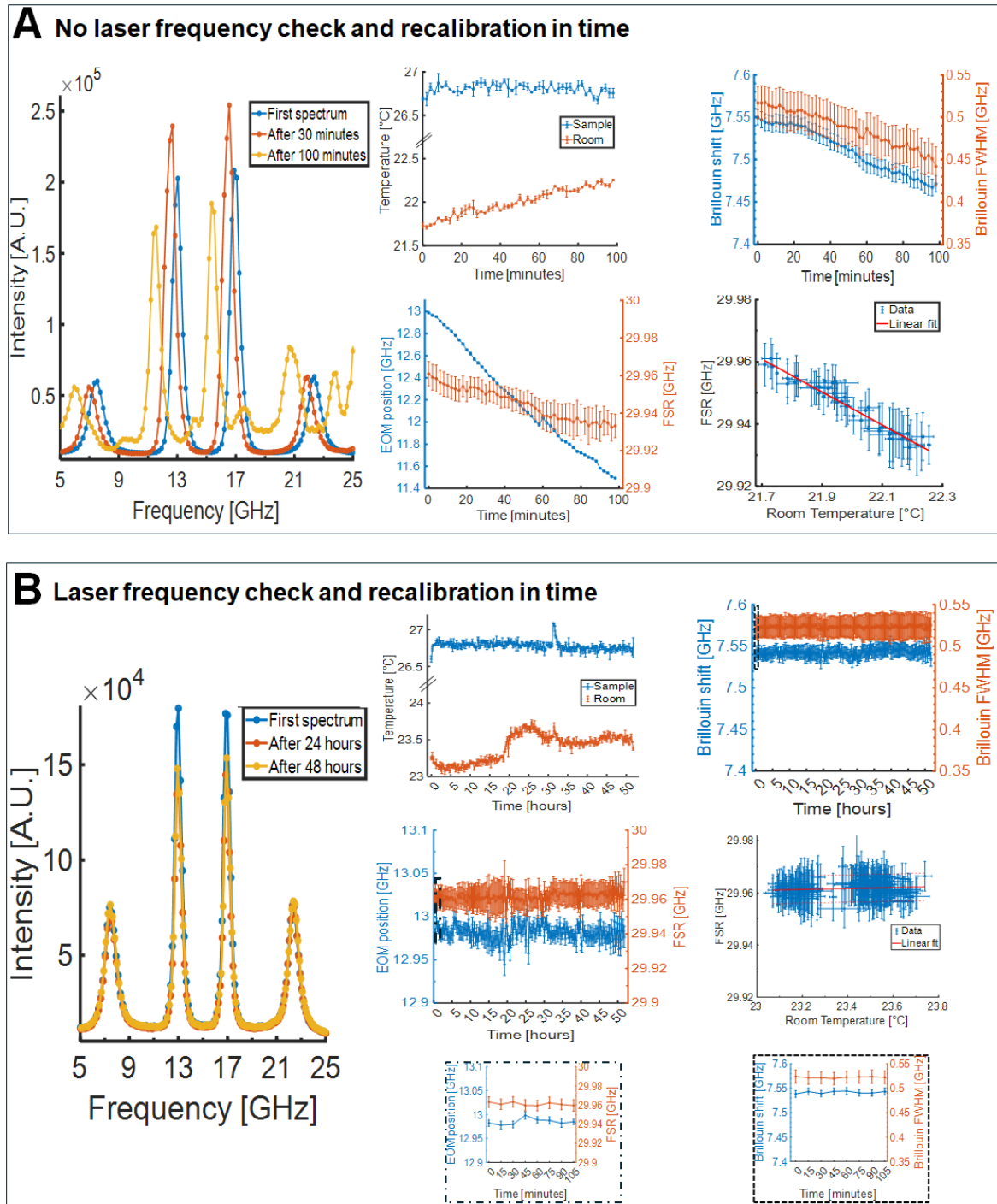


Figure 4: A Brillouin Microscope equipped with an EOM source (as calibrator and reference) and a tuneable laser shows superior stability in time. A: first panel: when the EOM is switched on, it is possible to quantify the drifts induced by room temperature changes; here we show 3 water Brillouin spectra acquired at different times with our double-VIPA setup, showing the same drift seen in Figure 1B. Eventually, Rayleigh line appears and results in camera saturation, so the acquisition had to be stopped after 100' and the spectrometer realigned. **Second panel:** temperature changes in the sample (blue line, kept constant with an incubator) and room (showing $<1^{\circ}\text{C}$ random changes in 100'). **Third panel:** Brillouin shift (blue) and FWHM (red) changes of the same water sample, performed every 2'. Because of temperature drifts affecting the VIPA or the laser, ν_B and Γ_B do not stay constant as they should. **Fourth panel:** EOM position (blue data) drifts of 1.5 GHz in 100', while FSR (red data) slightly changes. **Fifth panel:** the FSR change is significantly dependent ($R = 0.99$) from room temperature changes because of VIPAs cavity thermal expansions (seen also in Figure 1C). **B: first panel:** when laser frequency check and calibration are performed (Supplementary Figure S2), the Brillouin spectra remain fixed in the same position for hours and even days. Unwanted Rayleigh signal never appeared, showing no harmful camera saturation. **Second panel:** temperature changes of the sample (blue data) and the room (red data) across the 50 hours of experiment. Sample temperature was kept

constant with an incubator. *Third panel:* Brillouin shift (blue data) and FWHM (red) in time, showing complete steadiness in time, as they should be. *Fourth panel:* the EOM position (blue data) changed less than 0.4%; because of frequent calibrations, FSR remained constant as well. *Fifth panel:* FSR did not show any dependency from room temperature. *Squared inserts:* EOM position, FSR, Brillouin shift and FWHM behaviour from 0 to 100; i.e. the same time-scale as panel A. All data are shown as mean \pm standard deviation (SD) performed over 500 repeated measurements acquired at a single time; time = 0 refers to the manual alignment of the spectrometer, where Brillouin peaks have the same intensity.

To overcome this major problem and obtain a more stable Brillouin Microscope, we took advantage of the possibility to tune our 532 nm laser in a narrow frequency range. The laser frequency check consisted in a feedback control in a closed loop (Pontecorvo, 2024) that checked the EOM Anti-Stokes peak position (acting as a fixed reference during time) every 15': if its position in pixels had shifted more than a threshold from the original, the laser source was tuned to bring it back and an automatic pixel-to-GHz calibration was performed; if not, the laser frequency was not moved. The procedure is sketched in **Supplementary Figure S2** and better described in the Methods (Pontecorvo, 2024).

To test the temporal stability of the Brillouin Microscope equipped with an EOM and with a laser frequency check during acquisitions, we performed a 50-hours run recording the Brillouin spectra of water by checking the EOM peaks position (here at $v_{\text{EOM}}=13$ GHz, resulting in 2 peaks at v_{EOM} and $v_{\text{EOM}} - \text{FSR} = 17$ GHz) every 15 minutes, shifting the laser if needed at the beginning of every new acquisition. Representative Brillouin spectra of the first, middle (after 24 hours) and last (after 50 hours) timepoint are shown in the first panel of **Figure 4B**. During such a long measurement, the external room temperature was changing ($<1^{\circ}\text{C}$) while the sample was kept at a fixed temperature (**Figure 4B second panel**); however, now the Brillouin shift and FWHM shifted less than 0.005 and 0.009 MHz (**Figure 4B third panel**), while the EOM position fluctuated less than 0.05 GHz from the initial value of 13 GHz (corresponding to a $\approx 0.4\%$ fluctuation, **Figure 4B fourth panel**). Importantly, with the frequency check and automatic recalibration of the system, the FSR of the VIPAs remained constant over time and became totally independent from external room temperature changes (**Figure 4B fifth panel**). Box inserts show the behaviour of the Brillouin Microscope on the same timescale as **Figure 4A**, from which its superior stability was clear. In such a manner, here we showed that the use of an EOM with a tuneable laser source in a double-VIPA configuration allowed to perform periodic laser frequency checks during measurements: starting from a Brillouin Microscope stable for less than 20 minutes, we passed to an instrument stable for 2 days from the spectrometer manual alignment (**Figure 4B**).

This data confirmed the reliability and stability of our system to subtle environmental temperature changes, through the use of the feedback control in a closed loop. In conclusion, its stability and ease of use already represents a step forward in Brillouin

Microscopes and allows a straightforward application in the experiments related to more complex biological applications.

3. Conclusions

Brillouin Microscopy is a novel label-free optical technique that allows for the measurement of a sample's mechanical properties with high spatial resolution, in a non-invasive and non-contact manner through the measurement of the Brillouin shift. For life science applications, state-of-the-art Brillouin Microscopes (BMs) require the Brillouin shift precision to be within 0.1% of its value; however, many BMs experience temporal instabilities, mainly caused by temperature fluctuations, which can affect their performance and lead to inconsistencies when comparing data collected on different days. A further challenge for standard BMs is the calibration of the spectrometer: the currently accepted protocol in the literature uses known Brillouin shifts of water and methanol to reconstruct the calibration curve, but this approach is highly influenced by external factors that are unrelated to spectrometer's performances. To address this issues, the common solution is to frequently (approximately every 30 minutes) and manually realign the spectrometer and perform repeated calibrations with reference materials.

In this study, we presented an innovative method to remove temporal instabilities of a standard BM by inserting an Electro-Optic Modulator (EOM). The EOM serves three main purposes, as it can be used: *i*) as a reference signal during long data measurements; *ii*) as a calibrator, allowing the reconstruction of the spectrometer dispersion curve with greater precision than the standard protocol, in an automatic pipeline and without the need for reference samples; *iii*) as a tool to detect and compensate for temporal drifts in the system, through a feedback control in a closed loop. We here showed that our BM, equipped with an EOM and a tuneable laser, was capable of automatically acquiring data for more than 2 days without the need for spectrometer realignment; retrieved Brillouin shifts and widths showed superior stability than standard BMs, remaining constant throughout hours of experimental acquisition.

Taking together, these results pave the way to the development of a prototype of an automated Brillouin Microscope that, once aligned, can autonomously collect data with high spectral precision for extended periods, ranging from hours to days.

4. References

- D'Annunzio, S., Santomaso, L., Michelatti, D., Bernardis, C., Vitali, G., Lago, S., Testi, C., Pontecorvo, E., Poli, A., Pennacchio, F., Maiuri, P., Sanchez, E., Genevieve, D., Petrolli, L., Tarenzi, T., Menichetti, R., Potestio, R., Ruocco, G., & Zippo, A. (2024). *Chromatin condensates tune nuclear mechano-sensing in Kabuki Syndrome by constraining cGAS activation*. <https://doi.org/10.1101/2024.05.06.592652>
- Fasciani, A., D'Annunzio, S., Poli, V., Fagnocchi, L., Beyes, S., Michelatti, D., Corazza, F., Antonelli, L., Gregoretto, F., Oliva, G., Belli, R., Peroni, D., Domenici, E., Zambrano, S., Intartaglia, D., Settembre, C., Conte, I., Testi, C., Vergyris, P., ... Zippo, A. (2020). MLL4-associated condensates counterbalance Polycomb-mediated nuclear mechanical stress in Kabuki syndrome. *Nature Genetics*, 52(12), 1397–1411. <https://doi.org/10.1038/s41588-020-00724-8>
- Handler, C., Testi, C., & Scarcelli, G. (2024). Advantages of integrating Brillouin microscopy in multimodal mechanical mapping of cells and tissues. *Current Opinion in Cell Biology*, 88, 102341. <https://doi.org/10.1016/j.ceb.2024.102341>
- Kabakova, I., Zhang, J., Xiang, Y., Caponi, S., Bilenca, A., Guck, J., & Scarcelli, G. (2024). Brillouin microscopy. *Nature Reviews Methods Primers*, 4(1), 8. <https://doi.org/10.1038/s43586-023-00286-z>
- Martinez-Vidal, L., Testi, C., Pontecorvo, E., Pederzoli, F., Alchera, E., Locatelli, I., Venegoni, C., Spinelli, A., Lucianò, R., Salonia, A., Podestà, A., Ruocco, G., & Alfano, M. (2024). Progressive alteration of murine bladder elasticity in actinic cystitis detected by Brillouin microscopy. *Scientific Reports*, 14(1), 484. <https://doi.org/10.1038/s41598-023-51006-2>
- Pontecorvo E., Ruocco G., Zhang L., Gala F., Zanini G. and Testi C. (2024). *SISTEMA PERFEZIONATO DI RIVELAZIONE BRILLOUIN 102024000005674. Italy patent (2024)*.
- Scarcelli, G., Polacheck, W. J., Nia, H. T., Patel, K., Grodzinsky, A. J., Kamm, R. D., & Yun, S. H. (2015). Noncontact three-dimensional mapping of intracellular hydromechanical properties by Brillouin microscopy. *Nature Methods*, 12(12), 1132–1134. <https://doi.org/10.1038/nmeth.3616>
- Testi, C., Fasciani, A., Pontecorvo, E., Gala, F., Zippo, A., & Ruocco, G. (2021). MLL4 protein tunes chromatin compaction and regulates nuclear mechanical stress. In K. V. Larin & G. Scarcelli (Eds.), *Optical Elastography and Tissue Biomechanics VIII* (p. 4). SPIE. <https://doi.org/10.1117/12.2583238>
- Zhang, J., & Scarcelli, G. (2021). Mapping mechanical properties of biological materials via an add-on Brillouin module to confocal microscopes. *Nature Protocols*, 16(2), 1251–1275. <https://doi.org/10.1038/s41596-020-00457-2>

5. Acknowledgments

This research was funded by grants from ERC-2019-Synergy Grant (ASTRA, n. 855923); EIC-2022-PathfinderOpen (ivBM-4PAP, n. 101098989); Project “National Center for Gene Therapy and Drugs based on RNA Technology” (CN00000041) financed by NextGeneration EU PNRR MUR—M4C2—Action 1.4—Call "Potenziamento strutture di ricerca e creazione di “campioni nazionali di R&S” (CUP J33C22001130001).

6. Materials and Methods

532 nm Brillouin Microscope equipped with EOM

Our custom-built 532 nm Confocal Brillouin Microscope (**Figure 2A**) consists of an inverted microscope (Olympus IX-73) coupled to a double VIPA-based spectrometer through single-mode optical fibers (Zhang & Scarcelli, 2021). The laser source is a continuous wave, single-mode, tuneable laser of 532 nm wavelength (Oxxius) coming out from a single-mode fiber and a collimator. Most of the laser signal is sent to the sample through a polarizing beam splitter (PBS), while a small part is picked up and launched to the fiber-integrated Electro-Optic Modulator (EOM) through another collimator. The EOM is an electro-optic phase-modulator (Jenoptik PM532) whose inputs are the laser source and a radio-frequency driver (Lytid) working with an amplifier (Mini Circuits ZVE-3W-183+); its output is an optical signal shifted in frequency from 0 to 15 GHz, injected through another collimator and a PBS into the collection single-mode fiber.

The 3D mechanical properties of the sample are recovered in confocal laser scanning mode thanks to a pair of galvanometric mirrors (THORLABS) and a piezo stage (MadCity Labs), already described elsewhere (Martinez-Vidal et al., 2024). To arrive on the sample and retrieve its Brillouin spectra, the laser passes through a polarizing beam splitter, the galvo mirrors, a quarter wavelength plate and then is focused on the sample plane via an objective, working in backscattering configuration to ensure minimum spectral broadening. The retrieved Brillouin signals, scattered from a specific point of the sample, are then coupled to the collection single-mode fiber, whose core (diameter=3.2 micron) acts as a pinhole and allows for confocal sectioning of the sample. In the same collection fiber, the EOM signal is present as well and is sent to the spectrometer together with the Brillouin signal coming from the sample.

The spectrometer is composed by two orthogonal VIPAs (LightMachinery), both of Free Spectral Range (FSR) equal to 30 GHz. At the end of the spectrometer, an emCCD camera acquires the Brillouin spectra. We adjusted the VIPA angle to allow the transmission of a

couple of adjacent orders of Brillouin peaks (sketched in the lower panel of **Figure 1A**): when the spectrometer was correctly aligned, our Brillouin spectra showed 2 Brillouin peaks (a Stokes and Anti-Stokes signal per Rayleigh order) of equal intensity.

An automatic shutter (shown in **Figure 2B** as element G) blocks the signal coming from the sample and allows for automatic pixel-to-GHz calibration of the system during data acquisition, without interference from the Brillouin signal of the sample.

Aside from the Brillouin laser-scanning module, standard brightfield and fluorescence units (XLIGHT V1, Crest Optics) are located in the Microscope to retrieve morphological and fluorescence information of the sample.

The setup is controlled in MATLAB via a custom-built graphical user interface that, while acquires the data, checks the laser frequency drifts, performs pixel-to-GHz calibrations and governs the EOM frequency, as described in **Figure 3**.

The spectral precision of the microscope was between 8 and 10 MHz, obtained with the 4x (NA=0.11) at 100 ms and 15 mW power on the sample plane, measured with water Brillouin shift's distribution standard deviation. The signal-to-noise ratio was 30, calculated as the Brillouin water spectrum average intensity of the maximum divided by the standard deviation of the same point.

532 nm Brillouin Microscope acquisition of water (Figure 1B, 4A and 4B)

We acquired water data over a long period (a total of 60' in Figure 1B, 100' in Figure 4A, 52 hours in Figure 4B) with a 4x objective (NA = 0.11, Olympus) to ensure minimal broadening and shift of the Brillouin peaks (whose dependence from the objective NA is shown in **Supplementary Figure S1**). Water sample was maintained at a constant temperature of 27°C by using an incubator (Okolab).

All the data acquisitions followed the same protocol (sketched in **Supplementary Figure S2**) apart from the optional laser frequency check. Briefly, at time = 0 we aligned the spectrometer on the water signal, thus ensuring that the Stokes and Anti-Stokes Brillouin peaks of water were at the same height. We then performed pixel-to-GHz calibration by using different EOM frequencies (centered at $\nu_{EOM} = 7$ GHz, 8.7 GHz, 10.9 GHz and 11.5 GHz, as described in **Figure 3A** and **Figure 3B**), acquired 500 spectra of water by using an exposure time of 100 ms per point and an optical power on sample plane of 15 mW, for a total of ~1' acquisition.

We then paused the acquisition (the shutter was closed so that the laser could not induce sample heating) and waited $T=2'$ (**Figure 4A**), $10'$ (**Figure 1B**) or $15'$ (**Figure 4B**) to cyclically perform another one. At time = T, with the shutter closed, in data shown in **Figure 4A** we

performed the laser frequency check on the Anti-Stokes EOM peak (here centred at $v_{EOM} = 13$ GHz) and checked its pixel position, transformed in GHz with the reference calibration performed at the beginning: if it moved more than 100 MHz from the initial one, we moved the laser frequency accordingly until their difference was lower than 100 MHz and performed another calibration to prevent FSR changes; if not, we didn't move the laser frequency (in **Figure 4A**, this was always the case). After this, we opened the shutter and begin a new acquisition of 500 spectra on water, thus ensuring that the EOM was always centered at $v_{EOM} = 13$ GHz. We repeated this scheme N times: a total of N=6 times for data shown in **Figure 1B**, N=50 for **Figure 4A**, and N=208 for **Figure 4B**.

While acquiring Brillouin data, a PT100 was used as a temperature sensor in the sample and in the air.

Data shown in **Figure 1A** were performed with the same pixel-to-GHz calibration obtained with EOM frequencies, but during the acquisition the EOM frequency was blocked and no laser frequency check was performed.

780 nm Brillouin Microscope water data acquisition (Figure 1C)

The custom-built 780 nm Confocal Brillouin microscope is an inverted Nikon Microscope that uses a continuous-wave 780 nm laser source (TOPTICA), locked on the Doppler-free absorption line of Rubidium 85. The linewidth of Doppler-free absorption line is around 6 MHz. A homemade optical filter consisting of a Fabry-Perot (FP) crystal cavity and a Bragg grating is used to clean the incident light from amplified spontaneous emission noise and spurious cavity modes. The beam then is further cleaned with a spatial filter (a pinhole of 10 microns) which is placed in between two lenses, forming a telescope system to enlarge the beam, in order to fill the pupil of the microscope of the objective.

The sample is placed on a piezo stage (PRIOR) with x-y scanning capability. The backscattering light is also picked up through a fiber, allowing for confocal sectioning of the sample. Unlike the green setup, here the Brillouin spectrometer is based on a single VIPA setup (of Free Spectral Range FSR = 15 GHz, LightMachinery), where the elastic scattering light is suppressed by a Rubidium gas cell as a filter whose length is 7.5 cm. The setup is controlled in MATLAB via a custom-built graphical user interface.

We acquired water data over a long period (a total of 220' in **Figure 1C**) with a 10x objective (NA = 0.11, Nikon) to ensure minimal broadening and shift of the Brillouin peaks. As in the 532 nm water data acquisition, water was maintained at a constant temperature of 27°C by using an incubator (Okolab). At time = 0 we aligned the spectrometer on the water signal, thus ensuring that the Stokes and Anti-Stokes Brillouin peaks of water were at the same height. We then performed pixel-to-GHz calibration by

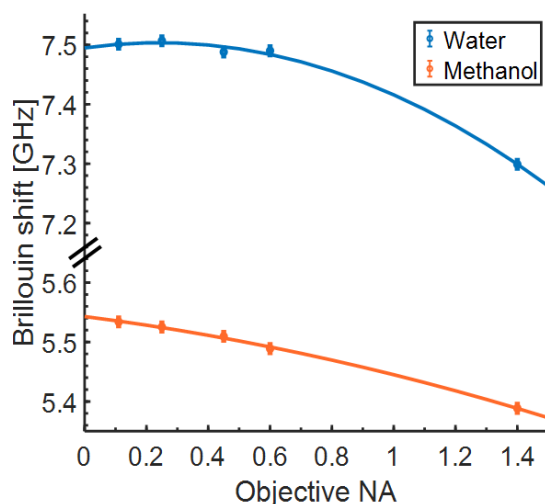
locking the laser at different Rubidium absorption frequencies (thus ensuring a reference-free calibration as in the 532 nm Brillouin Microscope) and acquired 500 spectra of water with an exposure time of 100 ms per point and an optical power on sample plane of 65 mW, for a total of ~1' acquisition. We then paused the acquisition and waited T=6' to cyclically perform another one, for a total of 35 acquisitions. While acquiring Brillouin data, a PT100 was used as a temperature sensor in the sample and in the air.

Brillouin Spectra Fitting

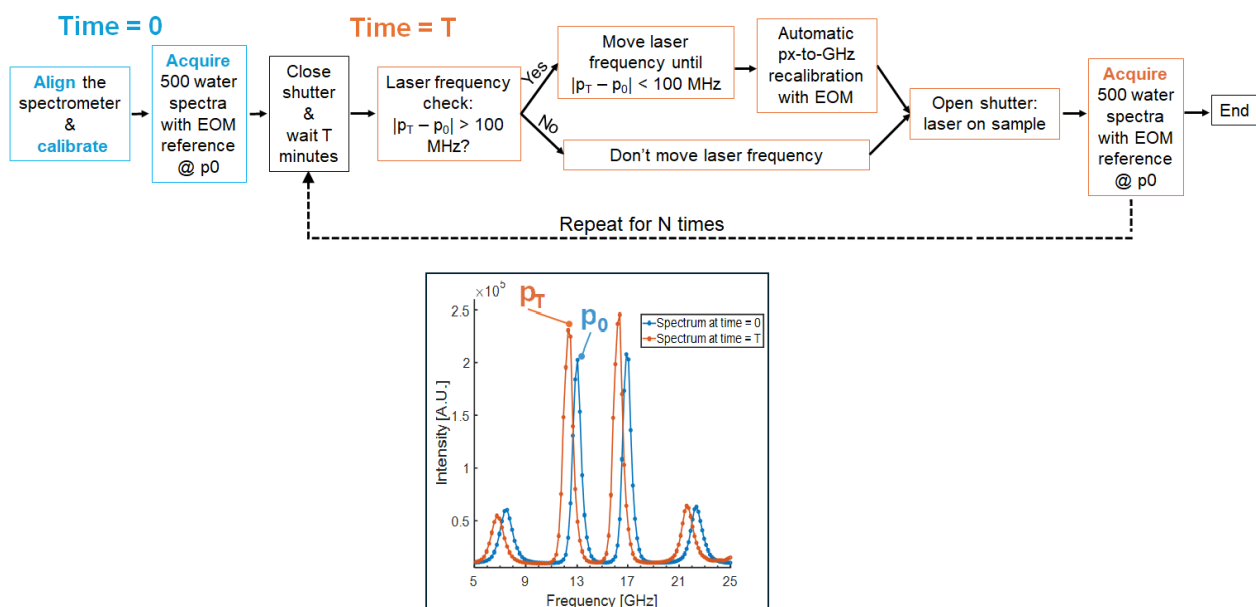
For 532 nm Brillouin Microscope, we fitted the sample's Brillouin signals with a sum of Lorentzians, while the EOM peaks with a sum of Gaussians. For 780 nm Brillouin Microscope, we fitted both Rayleigh and Brillouin signals with a sum of Lorentzians. For obtaining the Brillouin FWHM, we deconvolved the Brillouin signals with the spectrometer point spread function, thus obtaining a reliable Brillouin linewidth not affected by VIPAs broadening.

All the results shown in the graphs are given as mean \pm standard deviation (SD).

Supplementary Information



Supplementary Figure S1: Dependence of the Brillouin shift from the objective NA for the different materials used. Calibration materials as water (blue curve) and methanol (red curve) show a different dependence from the NA of the objective used. These frequencies values have been obtained with our innovative pixel-to-GHz calibration that is very precise and reliable. The Brillouin shift values imposed in the pixel-to-GHz calibration that uses water and methanol as calibrators (shown in **Figure 1D** and **Figure 3C**) are 7.50 GHz for water and 5.50 GHz for methanol: these have been extracted from theoretical considerations and are not true at high Nas; they also show temperature dependence. Data = mean \pm SD performed on 500 measurements.



Supplementary Figure S2: scheme of the water data acquisition performed in Figures 1B, 4A and 4B. At time = 0 we aligned the spectrometer on the water signal, thus ensuring that the Stokes and Anti-Stokes Brillouin peaks of water and EOM had the same intensity (blue spectrum of the lower panel); in this configuration, we performed pixel-to-GHz calibration by using different EOM frequencies (described in Figure 3A and Figure 3B). We then acquired 500 spectra of water for a total of $\sim 1'$ acquisition. After that, we paused the acquisition (the shutter was closed so that the

laser could not induce sample heating) and waited $T=2'$ (Figure 4A), $10'$ (Figure 1B) or $15'$ (Figure 4B) to cyclically perform another one. At time = T , with the shutter closed, in data shown in Figure 4A we performed the laser frequency check on the Anti-Stokes EOM peak (here centred at $\nu_{EOM} = 13$ GHz) and checked its pixel position, transformed in GHz with the reference calibration performed at the beginning. If it moved more than 100 MHz from the initial one, we moved the laser frequency accordingly in a feedback control in a closed loop (Pontecorvo, 2024) until their difference was lower than 100 MHz; we then performed another calibration to prevent eventual FSR changes. If it didn't move, the laser frequency was not modified (in Figure 4A, this was always the case). After this, we opened the shutter and begin a new acquisition of 500 spectra on water (red spectrum of the lower panel), thus ensuring that the EOM was always centered at $\nu_{EOM} = 13$ GHz. We repeated this scheme N times: a total of $N=6$ times for data shown in Figure 1B, $N=50$ for Figure 4A, and $N=208$ for Figure 4B.